

Mass Accommodation of Water: Bridging the Gap Between Molecular Dynamics Simulations and Kinetic Condensation Models

Jan Julin,^{*,†} Manabu Shiraiwa,[‡] Rachael E. H. Miles,[§] Jonathan P. Reid,[§] Ulrich Pöschl,^{||} and Ilona Riipinen[†]

[†]Department of Applied Environmental Science and Bert Bolin Centre for Climate Research, Stockholm University, SE-10691 Stockholm, Sweden

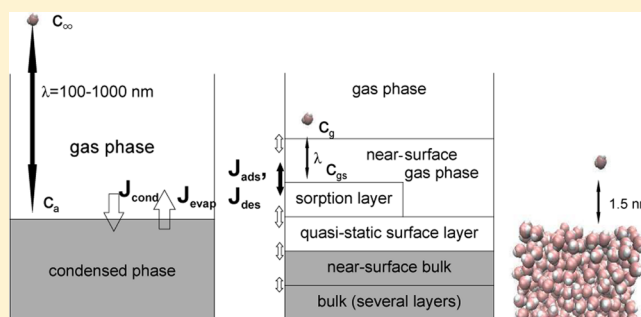
[‡]Division of Chemistry and Chemical Engineering, California Institute of Technology, Pasadena, California 91125, United States

[§]School of Chemistry, University of Bristol, Bristol, BS8 1TS, U.K.

^{||}Multiphase Chemistry Department, Max Planck Institute for Chemistry, P.O. Box 3060, 55128 Mainz, Germany

ABSTRACT: The condensational growth of submicrometer aerosol particles to climate relevant sizes is sensitive to their ability to accommodate vapor molecules, which is described by the mass accommodation coefficient. However, the underlying processes are not yet fully understood. We have simulated the mass accommodation and evaporation processes of water using molecular dynamics, and the results are compared to the condensation equations derived from the kinetic gas theory to shed light on the compatibility of the two. Molecular dynamics simulations were performed for a planar TIP4P-Ew water surface at four temperatures in the range 268–300 K as well as two droplets, with radii of 1.92 and 4.14 nm at $T = 273.15$ K.

The evaporation flux from molecular dynamics was found to be in good qualitative agreement with that predicted by the simple kinetic condensation equations. Water droplet growth was also modeled with the kinetic multilayer model KM-GAP of Shiraiwa et al. [*Atmos. Chem. Phys.* **2012**, *12*, 2777]. It was found that, due to the fast transport across the interface, the growth of a pure water droplet is controlled by gas phase diffusion. These facts indicate that the simple kinetic treatment is sufficient in describing pure water condensation and evaporation. The droplet size was found to have minimal effect on the value of the mass accommodation coefficient. The mass accommodation coefficient was found to be unity (within 0.004) for all studied surfaces, which is in agreement with previous simulation work. Additionally, the simulated evaporation fluxes imply that the evaporation coefficient is also unity. Comparing the evaporation rates of the mass accommodation and evaporation simulations indicated that the high collision flux, corresponding to high supersaturation, present in typical molecular dynamics mass accommodation simulations can under certain conditions lead to an increase in the evaporation rate. Consequently, in such situations the mass accommodation coefficient can be overestimated, but in the present cases the corrected values were still close to unity with the lowest value at ≈ 0.99 .



1. INTRODUCTION

Atmospheric aerosol particles influence the global climate through their two-fold impact on Earth's radiative balance. They scatter incoming solar radiation directly, but they also affect the climate indirectly by acting as condensation nuclei for cloud droplets (CCN), therefore affecting the radiative properties and lifetime of clouds.^{1,2} The CCN grow to become cloud droplets by condensation of water vapor, and this growth is controlled by the ability of the droplets to uptake the condensing water vapor molecules. Therefore an understanding of the underlying condensational growth process is necessary to achieve correct concentrations of cloud droplets in climate models.^{3–5} The key quantity controlling the growth of submicrometer aerosol particles is the mass accommodation coefficient α_m , which is defined as the fraction of vapor

molecules hitting the particle surface that will be accommodated by the condensed phase.^{6,7}

The mass accommodation of water molecules on water surfaces has been extensively studied both experimentally and with molecular dynamics (MD) simulations.^{8–21} However, the value of α_m reported by different experimental studies has varied in the range 0.01–1.^{8–11} A recent sensitivity analysis of results measured by a number of ensemble and single particle techniques has suggested that the values of the mass accommodation coefficients retrieved from these studies are consistent with a value larger than 0.5.¹³ The wide range of experimental values is contrasted by MD simulations which

Received: October 25, 2012

Revised: December 18, 2012

Published: December 19, 2012

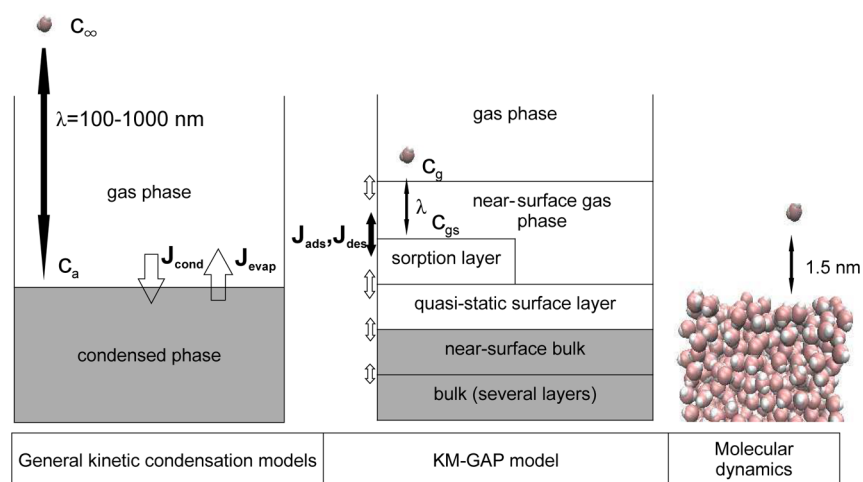


Figure 1. Schematic figure illustrating the different levels of theory from kinetic condensation models through KM-GAP to MD. The adsorption flux in KM-GAP (J_{ads}) is equivalent with the condensation flux of the general kinetic condensation model, and the KM-GAP desorption flux (J_{des}) is equivalent with the evaporation flux.

have consistently resulted in a unity mass accommodation coefficient for water.^{18–21} Part of the difficulty in determining the mass accommodation coefficient is linked to the fact that the coefficient can be defined in different ways. While the definition given above seems simple, the mass accommodation coefficient can be understood in at least two ways: either as surface accommodation where all molecules that are not directly scattered are considered to be accommodated or as bulk accommodation where mass accommodation is defined as the fraction of the molecules arriving at the surface that are absorbed to the bulk.⁶ The latter definition thus requires a separate definition of bulk and surface.

The experimental results on mass accommodation and evaporation are usually interpreted with the aid of various condensation models.^{7,22,23} These models are generally based on a combination of the kinetic gas theory and macroscopic mass and heat transfer theories. In this work we compare MD simulations to these kinetic condensation models to shed light on how compatible the two approaches actually are for the accommodation of water molecules onto water surfaces. One of the key complications in the interpretation of the laboratory experiments is that they always probe net condensation or evaporation processes, thus requiring quantification of simultaneous evaporation and condensation processes. MD simulations, on the other hand, provide a means to study these two processes separately, and at constant temperature.

Basic kinetic condensation models estimate the condensational flux from the kinetic theory of gases,¹¹ correcting for diffusional effects in the gas phase, where needed.⁷ The description considers the flux as occurring directly between the gas and condensed phases (see Figure 1) without any specific consideration of the processes occurring in the surface region. The condensational flux consists of molecules arriving at the surface from a distance that is of the order of the molecular mean free path λ . In these kinetic models the mass accommodation coefficient is present as the condensation coefficient, multiplying the maximum kinetic collision rate to the liquid surface. Based on the equality of the net condensation and evaporation fluxes in equilibrium, the condensation coefficient is typically considered to be equal to the evaporation coefficient.¹¹ As a next step from these simple theoretical considerations, more sophisticated models which

also explicitly include the surface processes have been presented.²⁴ Recently Shiraiwa et al. developed a new kinetic multilayer model for gas–particle interactions in aerosols and clouds (KM-GAP).²³ In KM-GAP the aerosol–gas system is divided into several layers (Figure 1), with corresponding fluxes between each layer. The mass accommodation coefficient is present as separately defined surface and bulk accommodation coefficients that appear as parameters of the model. MD simulations provide a means to investigate these descriptions of the condensation/evaporation process on a molecular basis (Figure 1).

MD simulations provide a straightforward way to determine α_m as the trajectories of individual molecules can be followed throughout a simulation and the fraction of accommodated molecules can be simply evaluated. The MD mass accommodation simulations consist of shooting individual gas phase molecules toward a surface and determining the subsequent fate of those molecules (see section 2.4). To our knowledge, so far in pure water mass accommodation MD the surface in question has always been a planar surface. At typical atmospheric conditions, however, only the growth of the smallest nanodroplets (of submicrometer size) are in fact sensitive to mass accommodation processes.¹⁰ Droplets in the few-nanometers range are accessible for present-day MD, and the surface curvature could have an effect on the mass accommodation process, being especially important for small atmospheric droplets. We study the potential effect of surface curvature by conducting MD simulations on the accommodation of water on nanodroplets and comparing the results to similar simulations for a planar surface.

A further complication related to a MD mass accommodation coefficient, and in fact to a molecular level α_m in general, is the fact that a fraction of the evaporating molecules observed during the mass accommodation simulations can be due to the incoming molecules inducing an “exchange evaporation” of a surface molecule.^{18,25} If this phenomenon has a nonnegligible effect, the assumed equality of the condensation and evaporation coefficients may not hold. While the exchange evaporation cases should also be considered as nonaccommodation, lacking any clear temporal and spatial definition on when the evaporation is induced by the incoming molecules, it is impossible to assign an individual evaporation event to either

exchange or thermal evaporation. However, the thermal evaporation rate is independent of the properties of the surrounding vapor phase, and it can be determined by simulating evaporation from the liquid into a vacuum.²⁶ We compare the evaporative flux into a full vacuum with that of a mass accommodation simulation to yield estimates on what fraction of the evaporated molecules should be counted as exchange evaporation—and thus inducing a feedback between the condensation and evaporation processes.

2. METHODS

2.1. Molecular Dynamics Simulation Details. The MD simulations were performed using the GROMACS molecular dynamics software.²⁷ The TIP4P-Ew water potential²⁸ was used. The simulation time step was 1 fs, the temperature was controlled through the Bussi thermostat,²⁹ and particle-mesh Ewald summation was used for the long-range part of the Coulombic interactions. The initial configurations consisted of either a liquid slab with the surfaces in the *xy*-plane and the simulation box elongated in the *z*-direction, or a liquid droplet located at the center of the simulation box. Periodic boundary conditions were used for all simulation boxes. The various simulation configurations are collected in Table 1. For each

Table 1. Various Simulation Setups of This Work^a

target surface	molecules	<i>T</i> (K)	droplet radius (nm)	box dimensions (nm ³)
droplet	1000	273.15	1.92	10.0 × 10.0 × 10.0
droplet	10000	273.15	4.14	21.6 × 21.6 × 21.6
planar	1000	273.15		3.1 × 3.1 × 10.0
planar	1000	268		3.1 × 3.1 × 10.0
planar	1000	290		3.1 × 3.1 × 10.0
planar	1000	300		3.1 × 3.1 × 10.0

^aThe number of molecules denotes the molecules in the target bulk liquid at the start of the simulation.

initial condition a total of 1000 incident molecules were generated at 10 ps intervals at a distance of about 1.5 nm from the target surface and were assigned velocities from the Maxwell–Boltzmann velocity distribution corresponding to the temperature in question. For the planar cases, the incident molecules were introduced at alternating sides of the slab at random *x,y*-coordinates and the center of mass velocity of the molecule was set toward the center of the surface. Consequently, the procedure results in a variety of incident angles and orientations. For the droplet cases, the incident molecules were placed at randomly selected locations around the droplet and the initial velocity was set toward the center of mass of the droplet. After the generation of the tenth incident molecule the simulation was continued for a further 20 ps before the simulation was terminated and a new mass accommodation simulation was started with a fresh starting configuration. The total simulation time for a single condition was thus 11 ns, the setup following the steps of Morita et al.¹⁸ The necessity of restarts becomes especially clear in the case of the droplet simulations, as the droplet radius needs to be constant.

We have also performed simulations without the impacting molecules present, that is, simulations where the system only consists of the slab or droplet, in order to study the evaporation from the surface without incoming gas phase molecules affecting the situation. This is not a true vacuum case as the

evaporated molecules are allowed to travel across the periodic boundary of the simulation box and, thus, eventually return to the liquid. However, the resulting evaporation flux should represent a reasonable approximation of the evaporation flux to a true vacuum when considering the small amount of evaporating molecules in the studied temperature range. These runs were performed for 20 ns of simulation time for all conditions used in the mass accommodation simulation except for the larger droplet, which is omitted because of the relatively high computational cost of a 10 000 water molecule system.

2.2. Condensation Models. The kinetic gas theory can be used for modeling the net condensation/evaporation to/from an aerosol particle if the Knudsen number *Kn*, which is the ratio between the mean free path of the vapor molecules λ and the particle radius r_p , is considerably larger than 1. In this free molecular regime, the net condensational mass flux (in molecules per second) to a droplet with surface area *A* (m²) is thus given by^{30,31}

$$J_{\text{net,kin}} = J_{\text{cond,kin}} - J_{\text{evap,kin}} = A\alpha\frac{\bar{v}}{4}(c_{\infty} - c_a) \quad (1)$$

where \bar{v} is the average thermal velocity of a molecule (m/s), c_{∞} is the gas phase density (1/m³) far from the droplet (about one mean free path away and further), and c_a is the gas density at the droplet surface. The α here is the condensation coefficient, which is equal to the evaporation coefficient in an equilibrium case.¹¹ This equality is usually assumed to hold in general, thus yielding the form of eq 1, where the first term refers to the forward condensation flux to the particle and the second term refers to the evaporation from it. The condensation coefficient can also be called the mass accommodation coefficient, as it is by definition the ratio of the actual condensational mass flux and the collision flux. At this level of theory (see Figure 1), it is not possible to address whether the condensation coefficient requires that the colliding molecule should end up in the bulk or merely stick to the surface as the surface is not treated explicitly.

Based on the collision flux and the requirement for the net flux between the gas and liquid phases to be zero at equilibrium, the evaporative flux from a surface with an area *A* is given by

$$J_{\text{evap,kin}} = \frac{p_e}{kT} \frac{\bar{v}\alpha}{4} A \quad (2)$$

where p_e is the equilibrium vapor pressure (Pa), k is the Boltzmann constant (J/K), and T is the temperature (K). Equation 2 is derived from considering an equilibrium situation between the condensed and vapor phases, but as the thermal evaporation rate is a property of only the condensed phase, the equation is usually assumed to be valid regardless of the vapor conditions above the surface.

As mentioned above, the free molecular regime equations hold if $Kn \gg 1$, while as the Knudsen number approaches unity and diminishes to values considerably less than 1, the flux expressions need to be corrected for gas phase diffusional effects. This is done in practice by multiplying the free molecular regime flux by a correction factor, yielding a general flux expression of the form

$$J_{\text{net}} = B J_{\text{net,kin}} \quad (3)$$

One of the most widely used transition regime correction factors was derived by Fuchs and Sutugin,³² and is given by (see, e.g., ref 7)

$$B = \frac{1}{1 + \alpha \frac{0.75 + 0.283Kn}{Kn(1 + Kn)}} \quad (4)$$

This factor follows from a fit to a numerical solution to the Boltzmann equation for a condition where the diffusing species is lighter than the background gas.

Figure 2a illustrates the kinetic collision flux density, that is $J_{\text{cond,kin}}/A$ with $\alpha = 1$, as a function of water vapor pressure. For

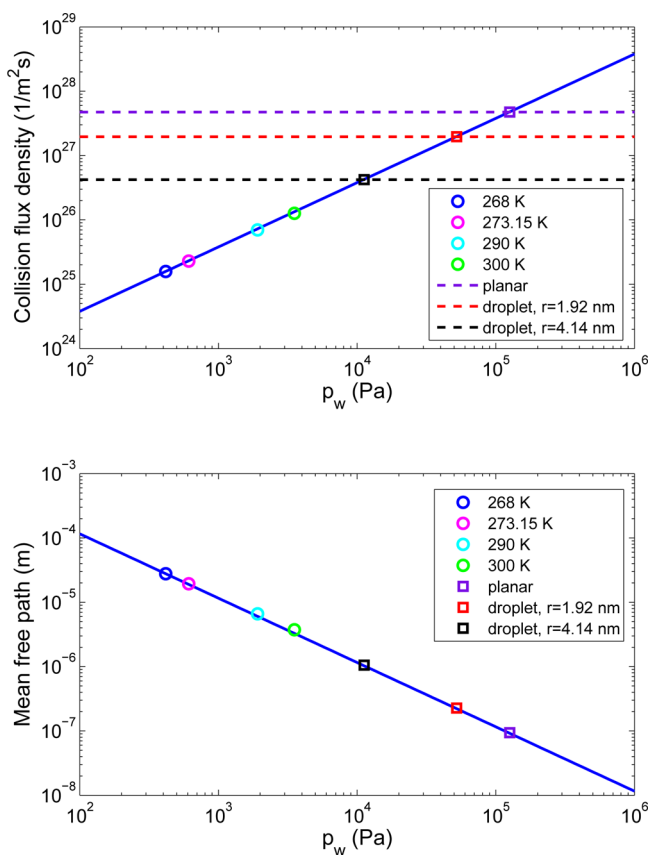


Figure 2. (a, top) Molecular flux density as a function of vapor pressure at $T = 268$ K. Other temperatures used in this work are omitted as they result in overlapping lines. The circles correspond to the equilibrium vapor pressure for the various temperatures. Dashed lines show the flux densities in the MD simulations. (b, bottom) Mean free path as a function of temperature. Circles correspond again to the equilibrium vapor pressures at the various temperatures, while the squares correspond to the MD simulation conditions.

the four different temperatures used in this study (268, 273.15, 290, and 300 K) the lines lie practically on top of each other, so for clarity only the line corresponding to the lowest temperature is included. The circles highlight the equilibrium vapor pressure for the different temperatures. The dashed lines show the flux densities corresponding to the conditions in our mass accommodation simulations, with the squares highlighting the corresponding pressures. As can be seen, the generation of incident molecules every 10 ps effectively corresponds to a range of very high supersaturations of ≈ 10 –200. Figure 2b shows the mean free path of water molecules as a function of pressure. Again, the lines corresponding to the three highest temperatures are omitted for clarity. The circles denote the equilibrium vapor pressures at our model temperatures, while the squares indicate the mean free paths corresponding to the “effective” pressure created by the incident molecules. As can be

seen, even with the relatively high supersaturations represented by these simulations the mean free paths are orders of magnitude longer than the 1.5 nm distance from where the incident molecules begin their trajectory to the surface. The corresponding Knudsen numbers for our simulated conditions are thus on the order of about 30 to a few hundred, thus justifying the use of the free molecular regime condensation equations for our comparisons. In general, there are two possible approaches to set up the mass accommodation MD simulations: the one employed here (and in, e.g., ref 18) where several molecules are generated before restarting, or restarting for every incident molecule (e.g., ref 21). Because of computational limitations, both necessarily represent a high ratio of collisions/simulation time and thus correspond to high supersaturations. In the latter case, however, the surface is refreshed and is thus not subject to continuous “bombardment”.

While the kinetic condensation models assume that the molecules arriving at the surface originate on average from the distance of the mean free path, creating the incident molecules in MD closer to the surface does not hamper the determination of the mass accommodation coefficient in any way; for this purpose only the fate of the molecules at the surface is needed, not the long journey beforehand.

2.3. Condensation in the KM-GAP Model. The KM-GAP model²³ is based on the kinetic model framework of Pöschl, Rudich, and Ammann²⁴ and treats explicitly the steps of mass transfer from gas to condensed phase including gas diffusion, surface–bulk exchange, and bulk diffusion of water molecules (see Figure 1). The model divides the gas phase and the bulk condensed phase into a number of layers, and the surface is described by two layers: the quasistatic surface layer and the sorption layer. The flux between the aerosol and the gas phase occur only between the sorption layer and the near-surface gas phase. Compared to the simplified picture of section 2.2 (Figure 1, left), where mass transfer is only described by the condensation and evaporation fluxes between the condensed and gas phases, KM-GAP adds a comprehensive set of additional fluxes to the picture with an additional pair of fluxes describing the transport between each layer (Figure 1). The transport from the near-surface gas phase to the first (near-surface) bulk layer is not only controlled by the condensational flux to the sorption layer, but also by the transport between the sorption and quasi-static surface layers and between the quasi-static surface layer and the near-surface bulk.

Determining the condensational flux to the surface in KM-GAP follows from the collision flux in the same way as for the simple kinetic models, and for gas molecules of a given species the collision flux is given by

$$J_{\text{coll}} = c_{\text{gs}} \frac{\bar{v}}{4} \quad (5)$$

where c_{gs} is the near-surface gas phase concentration of the species in question. Uptake of the gas molecules will cause a depletion in the near-surface gas phase, establishing a concentration gradient in the gas phase, and thus uptake will be influenced by gas phase diffusion. This is addressed by adjusting the concentration with a diffusion correction factor $B_g = c_{\text{gs}}/c_g$. Following the Fuchs and Sutugin transition regime correction, the correction factor is given by²⁴

$$B_g = \frac{1}{1 + \gamma \frac{0.75 + 0.28Kn}{Kn(1 + Kn)}} \quad (6)$$

where Kn is the Knudsen number and γ is the uptake coefficient, defined as the ratio of the net flux between the gas and the condensed phases (as defined by eq 1) and the collision flux. Finally, the adsorption flux (corresponding to the condensation flux in eq 1) in KM-GAP can be written as

$$J_{\text{ads}} = \alpha_s J_{\text{coll}} \quad (7)$$

where α_s is the surface accommodation coefficient.

The surface accommodation coefficient in eq 7 is formally identical to the definition of the condensation coefficient given in section 2.2. KM-GAP also provides a bulk accommodation coefficient α_b as an output parameter which describes the probability of a gas phase molecule entering the bulk. However, as outlined above, α_b does not enter the equations arising from gas phase kinetics in the KM-GAP treatment.

2.4. Determining the Mass Accommodation Coefficient in MD. Unlike the kinetic models where the mass accommodation coefficient appears in equations concerning mass fluxes, in MD the coefficient is determined by studying the fates of individual molecules arriving on a surface. The possible fates of gas phase molecules arriving at the surface can be roughly divided into four outcomes,^{19,20,33} which are scattering, desorption, adsorption, and absorption. Both scattered and desorbed molecules return to the gas phase, the difference being that desorbed molecules spend some time on the surface before doing so. Adsorbed and absorbed molecules remain in the liquid, with absorbed molecules ending up in the bulk liquid and adsorbed molecules on the surface. There are a few ways in which the mass accommodation coefficient can be defined with this classification. It is clear that the scattered molecules cannot be considered accommodated in any definition. Lacking any definite criteria on the time an incoming molecule has to stay on the surface, the definition for a surface accommodation coefficient is

$$\alpha_s = \frac{\text{number of incoming molecules that did not scatter}}{\text{all incoming molecules}} \quad (8)$$

This definition is in agreement with the surface accommodation coefficient as it appears in KM-GAP.

However, if the mass accommodation coefficient is understood as the fraction of incoming molecules that are absorbed into the bulk liquid, we might use the formula¹⁹

$$\alpha_b = \frac{n_{\text{absorb}} + p_k n_{\text{adsorb}}}{n_{\text{absorb}} + n_{\text{adsorb}} + n_{\text{desorb}} + n_{\text{scatter}}} \quad (9)$$

where the correction factor p_k is

$$p_k = \frac{n_{\text{absorb}}}{n_{\text{absorb}} + n_{\text{desorb}}} \quad (10)$$

This correction factor is introduced because the limited simulation time prevents following the trajectories of the adsorbed molecules until they are either absorbed or desorbed. In the case for water, both in our present work and in for example ref 19, no occurrences of desorption of the incoming molecules is observed. This makes the two definitions presented above identical over the time scales of our MD simulations.

From the classification above it is clear that these definitions consider only the fate of incoming molecules, and the possible exchange evaporation, that is, the evaporation of a surface molecule induced by an incoming molecule, is not taken into account. However, from the point of view of the mass fluxes to and from the surface, it is irrelevant if the outgoing molecule is the same as the incoming one. In principle the exchange evaporation could be taken into account in the above definitions by assigning to this new category what would otherwise be classified as absorption or adsorption, but the problem remains that these events would need to be distinguished from thermal evaporation governed by eq 2. Indeed, even performing a separate set of evaporation simulations to observe differences in the evaporation rate provides only an idea of the magnitude of this effect, not a way to classify individual evaporation occurrences.

3. RESULTS AND DISCUSSION

3.1. Evaporation Rates: Comparison of Kinetic Condensation Models and MD. The MD simulated evaporation rates for the planar surfaces are plotted as a function of temperature in Figure 3 for both the evaporation

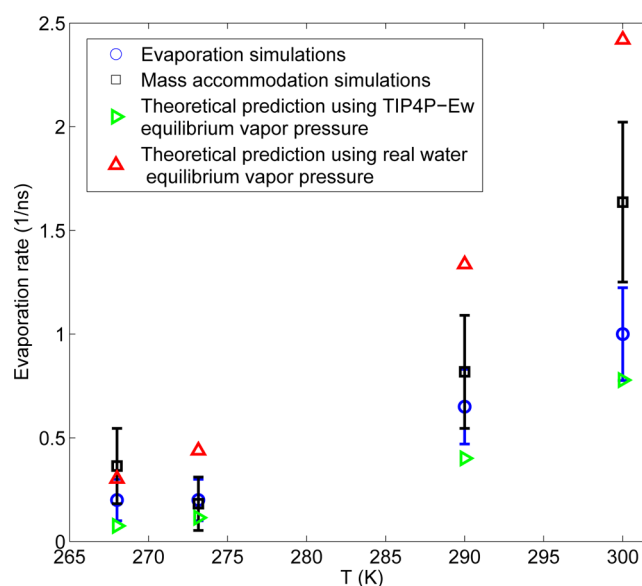


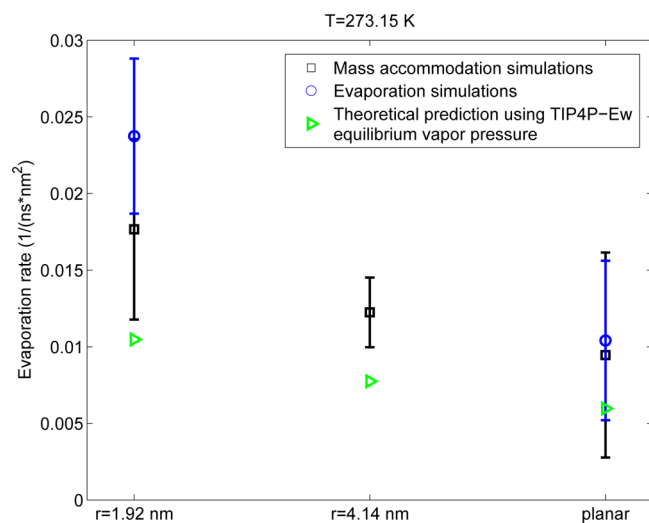
Figure 3. Evaporation rate as a function of temperature.

and mass accommodation simulations. For comparison, Figure 3 shows the theoretical prediction given by eq 2, with the equilibrium vapor pressures based on the simulated values for TIP4P-Ew water reported by Vega et al.³⁴ While Vega et al. report values for p_e down to 245.5 K, their reported fit for p_e with the form $\ln(p) = A + B/(T + C)$ is for temperatures above 300 K. We have therefore for our purposes fitted the lower temperature end (<400 K) of their simulated pressures using the same functional form. The values used are given in Table 2. The value for the mass accommodation, or evaporation, coefficient in eq 2 is set to 1. Figure 4 shows the evaporation rates for different droplet sizes at $T = 273.15$ K. The droplet radii given, 1.92 and 4.14 nm for the 1000 and 10 000 molecule droplets respectively, are the equimolar radii of the droplets. For equilibrium vapor pressures above a curved surface, the Kelvin effect must be accounted for, which requires knowledge of the liquid density and surface tension. We have used the

Table 2. Quantities Used To Calculate the Theoretical Predictions of Evaporation Rates in Figures 3–5^a

T (K)	p_e (Pa)	γ (mN/m)	ρ_l (kg/m ³)
268	103	–	–
273.15	159	67.8	997
290	572	–	–
300	1130	–	–

^aEquilibrium vapor pressures p_e from our fit to data from ref 34 (see text), and surface tension γ and liquid density ρ_l from ref 35.

**Figure 4.** Evaporation rate as a function of droplet size at $T = 273.15$ K.

recent values given by Sakamaki et al.³⁵ at 273 K for the TIP4P-Ew model. For convenience these values are also listed in Table 2.

For comparison, Figure 3 shows also the prediction of eq 2 when the equilibrium vapor pressure of real water is used.¹⁰ It should be stressed that for a meaningful comparison between simulated rates and the prediction of eq 2 one must look at the points obtained using the simulated p_e , not the experimental one.

In order to get an error estimate from the MD simulations, we note that the evaporation process is a Poisson process,²¹ and we calculate the 1σ error for the observed number of evaporation events during the total simulation time. If there is exchange evaporation taking place within the mass accommodation simulations, the observed evaporation is a combination of two processes and this error treatment is too simplified. The error bars shown are nonetheless found by treating both simulation sets in the same manner, since this will help clarify whether the differences seen could just be a product of the shorter simulation time in the mass accommodation simulations.

Figures 3 and 4 show that the theoretical evaporation rate from eq 2 results in values that are reasonably close to the evaporation rates seen in simulations. Moreover, the same qualitative behavior as a function of temperature and droplet size is seen in both simulation and theory. A notable exception would appear to be the dip seen when going from 268 to 273.15 K in the mass accommodation simulations. However, considering both the theoretically expected evaporation rates that are quite close to each other for the two temperatures and the relatively large and overlapping error bars which follow

from the small number of evaporation events (see Table 3), it is strongly suggested that the dip follows from poor statistics rather than an actual feature of the temperature dependence of the evaporation rate.

Table 3. Number of Evaporated and Scattered Molecules during Mass Accommodation Simulations

radius	T (K)	no. of scattered	no. of evaporated
1.92 nm	273.15	4	9
4.14 nm	273.15	2	29
planar	273.15	0	2
planar	268	0	4
planar	290	1	9
planar	300	2	18

The differences between the evaporation rates from mass accommodation and evaporation simulations appear to mostly be within statistical uncertainty for the lower temperatures, implying that the exchange evaporation does not have a significant role in these simulation conditions. For the higher temperatures, however, the evaporation simulations start to exhibit notably lower evaporation rates, remaining closer to the theoretical prediction which describes only thermal evaporation. It is therefore conceivable that a fraction of the evaporating molecules in the mass accommodation MD simulations at higher temperatures could be attributed to exchange evaporation. As was seen from Figure 2, the mass accommodation simulations correspond to very high supersaturations as a consequence of the relatively frequent generation of incident molecules. Thus, the assumption that the evaporation flux is independent of the condensation flux can be considered to be a good one for most, if not all, realistic natural situations for water. However, the exchange evaporation apparent in Figure 3 is notable only at the higher temperatures, which actually correspond to lower supersaturations than the lower temperature cases (see Figure 2). We conclude that the supersaturation where the effect becomes nonnegligible is temperature dependent, and the importance of exchange evaporation for other types of molecules should be further investigated.

Although the agreement between theory and simulation is fairly good (within a factor of ~ 2), the theoretical prediction consistently underestimates the simulated evaporation rate. The error bars in the simulated values are of course quite large, but the sensitivity of eq 2 to the input values should also be considered. As α is already set to 1, changing the value of the evaporation coefficient will only make the agreement worse (i.e., the value cannot exceed unity). Our MD simulations are thus in line with an evaporation coefficient of unity. The temperature and surface area are fixed in the simulations, so we are left with a possible underestimation of p_e as a source for the discrepancy. In Figure 5 the equilibrium vapor pressures of Vega et al.³⁴ are compared to values obtained by solving p_e from eq 2 using the MD simulated evaporation rate. We stress that the validity of the equilibrium vapor pressures of Vega et al.³⁴ is not questioned, Figure 5 merely illustrates the change in p_e that would be required to have the simulated and theoretical evaporation rates in Figures 3 and 4 agree. The equilibrium vapor pressure obtained through eq 2 is off by a factor of 2.7 for $T = 268$ K and by less than a factor of 2 for the other temperatures, equivalent to a difference of a few hundred pascals. The error bars are also in the range of a few hundred

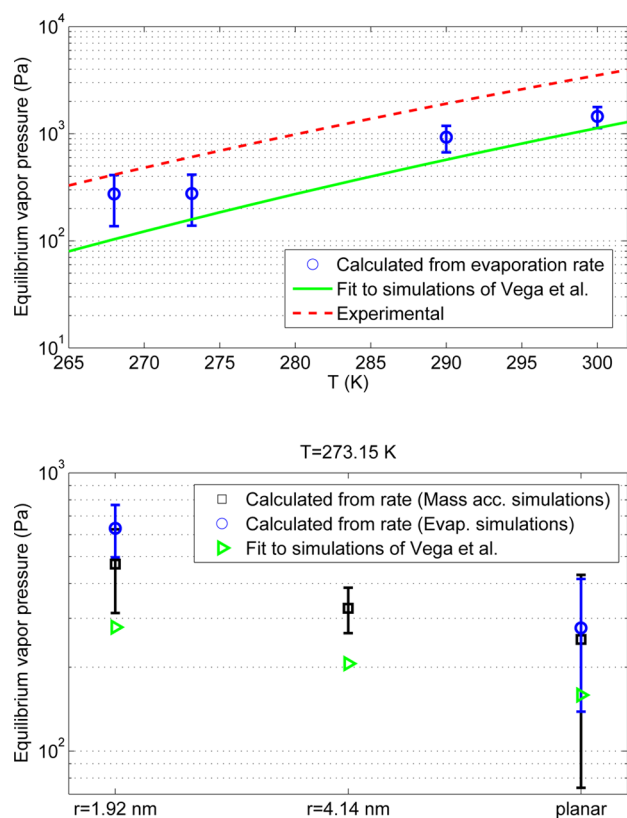


Figure 5. Comparison of simulated equilibrium vapor pressure of TIP4P-Ew water with approximated value obtained through the evaporation rate.

pascals, but as the pressures from eq 2 result consistently in an overestimation, it is unlikely that a longer simulation time and improved evaporation statistics would result in the vapor pressures coming into better agreement.

For the droplet cases, errors in the surface tension and bulk liquid density might also explain some of the disagreement between the theoretical and simulated evaporation rates. For the value of surface tension an error estimate of 0.4 mN/m has been given,³⁵ which translates to about a 0.5 – 1 Pa uncertainty in the droplet p_e . No error estimates were given for the liquid density, but even when considering a very generous error estimate of 10 kg/m³, a change in p_e of only about 0.5 – 1.5 Pa would result. Thus, the errors in surface tension and bulk liquid density do not improve the consistency between theoretical and simulated evaporation rates for the droplets.

3.2. KM-GAP Sorption Layer and Desorption Lifetime.

The surface region can be identified from a density profile in a MD simulation as the part where the density changes from the bulk liquid value to the gas phase value; see Figure 6. As a more rigorous definition for the surface, the region where the density is between 90 and 10% of the liquid value is commonly used.^{19,36} This “90–10” region is denoted by the red lines in Figure 6. The KM-GAP model²³ on the other hand describes the surface with two layers, the quasistatic surface layer and the sorption layer (see Figure 1). The rate of evaporation is described by the desorption lifetime τ_d , which is the mean time an evaporating molecule spends in the sorption layer before evaporating into the gas phase. As a test case in ref 23, the KM-GAP model was used to simulate the experimental water vapor condensation and droplet growth in the expansion chamber work of Winkler et al.¹⁰ In their experiments, monodisperse Ag

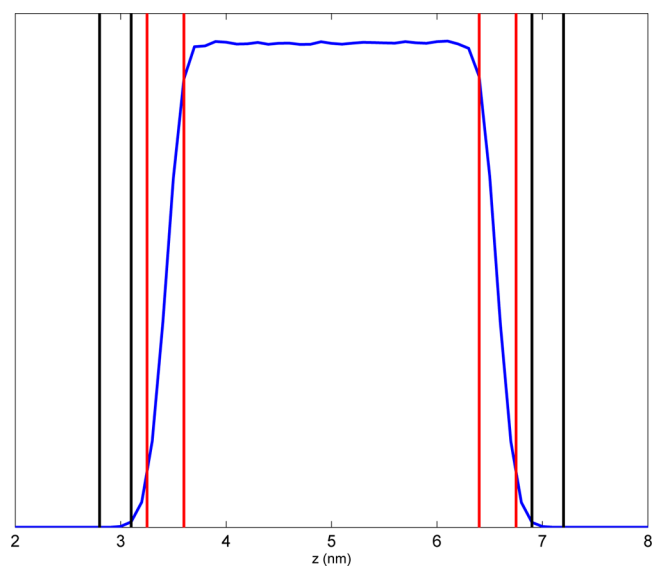


Figure 6. Example density profile ($T = 300$ K) where the area between black vertical lines is the KM-GAP sorption layer. The red lines denote where the density falls to 90% and 10% of the bulk liquid value.

particles with a diameter of 9 nm and particle number concentration of 4381 cm⁻³ were used as condensation nuclei and humidified under an initial supersaturation of 37.5% at 268 K and 737 Torr. A value of $\tau_d = 35$ ps was used in ref 23 for the desorption lifetime, based on earlier MD simulations.^{19,36} The value is, however, based on only a handful of desorption events of incoming molecules, of which not all were water molecules, and which were obtained using the 90–10 surface definition.

To identify where the location of the sorption layer is in terms of the MD density profile, we take advantage of the quantity denoted by θ_s in the KM-GAP model. θ_s is the ratio between the actual surface concentration of the sorption layer and the maximum surface concentration of water molecules. We take the outer limit of the sorption layer to be located at the distance where the density has fallen to the fraction of the corresponding bulk liquid value that is indicated by θ_s , which for the water condensation example in ref 23 is $\theta_s \approx 7 \times 10^{-5}$. The thickness of the sorption layer is set to 0.3 nm, since in KM-GAP the sorption layer has a fixed width of one molecular diameter. The black lines in Figure 6 show the region of the MD density profile that corresponds to the KM-GAP sorption layer. As can be seen, the outer limit of the sorption layer is quite far from the bulk liquid phase and the sorption layer lies entirely outside the 90–10 surface region. This was to be expected, as the KM-GAP surface region includes also the quasi-static surface layer located between the sorption layer and bulk condensed phase. Due to the dense vapor that follows from the frequently generated incoming molecules, the density does not fall in the mass accommodation simulations of the planar interface to the small value indicated by θ_s . This is however not a problem in the evaporation simulations, and the location identified from the evaporation simulations is used also for the mass accommodation simulations when calculating the τ_d related to the sorption layer.

Table 4 collects the values for the mean lifetime before evaporation when the 90–10 surface definition is used. The times the evaporating molecules spend in the surface are calculated starting from the last time the molecules enter the surface before evaporation without entering the bulk in

Table 4. Desorption Lifetime τ_d (Mean Value) When the Surface Follows the 90–10 Definition, and Also Median, Minimum, and Maximum Observed Desorption Lifetimes^a

radius	T (K)	mean (ps)	median (ps)	min (ps)	max (ps)	evaporations
1.92 nm	273.15	10.5 ± 10.5	5	1.5	38.5	30
4.14 nm	273.15	12.1 ± 8.7	9	2	35	27
planar	273.15	14.9 ± 12.7	12.5	2	36	6
planar	268	5.8 ± 6.3	3	1	19	8
planar	290	7.5 ± 5.9	5.5	1.5	24	22
planar	300	6.2 ± 3.9	5.5	1.5	16.5	38

^aThe number of events listed here is not exactly the same as the total number of evaporations since on three occasions the molecule was in the surface from the start of the simulation until evaporating.

between. Evaporation is here taken to occur when the molecule enters the constant density vapor phase. We find that, while individual evaporating molecules occasionally spend 35 ps or even longer in the 90–10 surface region, the mean lifetime is around 10 ps or less. To be consistent with KM-GAP, τ_d should be calculated using the sorption layer. This results in a τ_d that is on average below 1 ps for all of the various simulated conditions. The longest time observed is only about 2 ps, but these are a minority among the evaporation events with only six such occurrences among the total number of 134 evaporation events observed throughout all of the simulations.

To examine the effect of the value of τ_d on the predictions of KM-GAP, we have simulated water vapor condensation using KM-GAP with various τ_d values, again in comparison to experimental data from Winkler et al.¹⁰ We investigate the impact of τ_d on droplet growth with τ_d values of 1, 10, and 100 ps. The surface accommodation coefficient is set to 1. Figure 7 shows the results of such simulations. As shown in Figure 7a, KM-GAP reproduces the observed growth very well and the exact value of τ_d has practically no effect on particle growth. This is because particle growth is limited by gas phase diffusion and subsequent surface accommodation. However, τ_d does have a critical effect on the surface coverage of water molecule θ_s as shown in Figure 7b. Increase of τ_d by an order of magnitude leads to roughly an order of magnitude increase in θ_s : θ_s is $\approx 2 \times 10^{-6}$ with $\tau_d = 1$ ps, increasing to $\approx 2 \times 10^{-4}$ with $\tau_d = 100$ ps.

Figure 7c shows the temporal evolution of the surface and bulk mass accommodation coefficients (α_s and α_b) and uptake coefficient (γ). α_s stays at 1 whereas $\alpha_b \approx 0.998$, which means that about 99.8% of water molecules that collide with the surface eventually enter the bulk. The almost exact agreement between the values of α_s and α_b indicates that the transport of water molecules from surface to bulk is a very fast process due to the high bulk diffusivity of water molecules of $\sim 10^{-6} \text{ cm}^2 \text{ s}^{-1}$. γ drops from 1 to ~ 0.1 very quickly and afterward continues decreasing to ~ 0.01 , corresponding to a slowing down of particle growth. Water molecules are always desorbing from the surface, and the balance between adsorption and desorption of water molecules determines the γ value. As time progresses, the net flux decreases and the uptake coefficient decreases. Thus, for water, the surface and the bulk accommodation coefficient values as predicted by KM-GAP are nearly identical, and the problem reduces to the simple kinetic condensation problem.

When identifying the equivalent of the KM-GAP sorption layer within the MD simulations, we used the value of the sorption layer surface coverage θ_s taken from the KM-GAP runs of ref 23. Figure 7b shows, however, that the value of θ_s changes when τ_d is changed, and the location of the sorption layer should be moved accordingly. This makes it impossible to determine a definite location for the sorption layer in MD, and

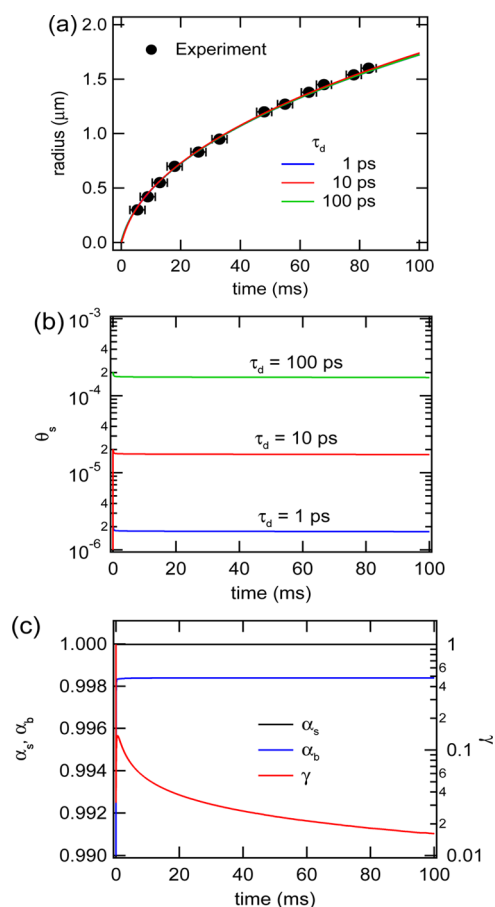


Figure 7. Temporal evolution of water vapor condensation simulated by KM-GAP. (a) Water droplet growth curve with different desorption lifetimes of H₂O (τ_d) (1, 10, and 100 ps) in comparison with the experimental data by ref 10. (b) Surface coverage of H₂O. (c) Surface and bulk mass accommodation coefficients (α_s and α_b ; left axis) and uptake coefficient of H₂O (γ ; right axis) with $\tau_d = 1$ ps.

therefore also τ_d : a new value of τ_d will then again change the value of θ_s calculated from KM-GAP. In practice, however, we can be quite confident that τ_d should be around 1 ps. While they are orders of magnitude different from each other, all of the θ_s values seen in Figure 7b are small. Thus, when used to determine the MD equivalent of the sorption layer, each results in a sorption layer located close to the bulk gas and completely outside the 90–10 surface region. Then, for any of these values of θ_s , the sorption layer is located so far from the bulk liquid that an evaporating molecule in a MD simulation will not spend more time in the sorption layer than is required to cross it, of the order of 1 ps.

The introduction of the MD equivalent of the KM-GAP sorption layer was done here for the purpose of connecting the MD picture to KM-GAP terminology, and therefore the MD sorption layer is utilized only in this section.

3.3. Mass Accommodation Coefficient. Using eq 9 to determine the mass accommodation coefficient requires one to choose a definition for the surface. For this purpose we adopt the 90–10 definition (Figure 6), which is consistent with previous mass accommodation MD work. We find that the water mass accommodation coefficient, as defined by eq 9, is close to unity not only for the planar surfaces but also for the droplet surfaces, as is seen in Figure 8. The number of scattered

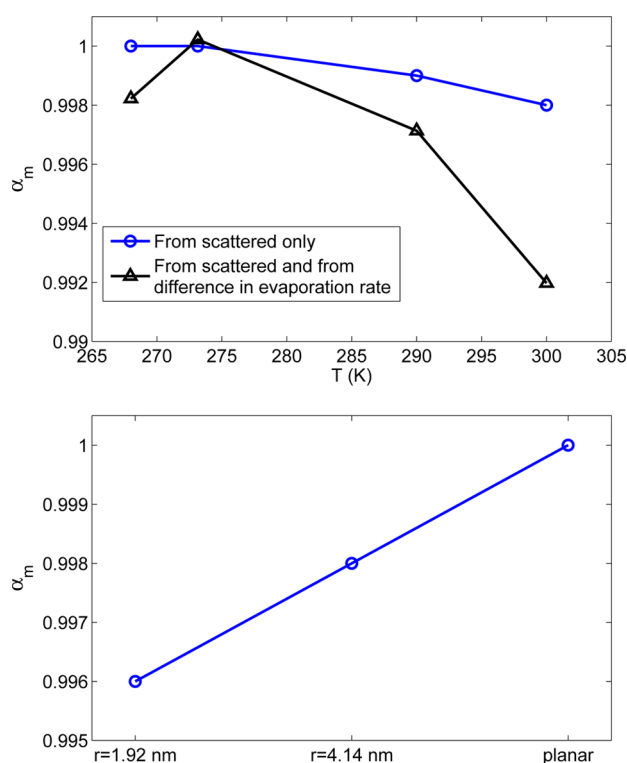


Figure 8. Mass accommodation coefficient as a function of temperature (top) and droplet size (bottom). The circles in the top follow from only counting scattered molecules as nonaccommodated; the triangles take also into account the difference in evaporation rate between mass accommodation and evaporation simulations.

molecules is particularly small (see Table 3), to the extent that we see no scattered molecules among the 1000 incoming molecules for the planar surface in simulations at the two lowest temperatures. The triangles in Figure 8 are calculated when taking the exchange evaporation into account where the number of evaporated molecules that are assigned to the exchange evaporation are determined from the ratio of evaporation rates from the evaporation and mass accommodation simulations. For completeness the results using the exchange evaporation are plotted also for the two lower temperatures, even though the difference in evaporation rates could clearly be accounted for by statistical error in these two cases (see Figure 3). There seems to be a slight decrease in α as the temperature grows and a slight increase as the droplet size grows. The decreasing trend as temperature rises is in line with earlier experimental results^{8,9,37} and with simulation results.^{26,38} This behavior is also predicted by transition state theory.³⁸ This behavior is intuitively expected as higher temperature

corresponds to on average more energetic incoming molecules. Note that the region where the accommodation coefficient drops to values considerably below unity in refs 26 and 38 is at temperatures close to the critical temperature, that is, at temperatures much higher than those in the present study or in experiments.^{8,9,37}

The mass accommodation coefficient remains practically unity even when the exchange evaporation is taken into account. However, it is interesting to note that for $T = 300$ K the number of nonaccommodated molecules due to exchange evaporation is about 4 times the number of scattered molecules, making the exchange evaporation the dominant type of nonaccommodation under these conditions. However, translating these findings to other substances with mass accommodation coefficients smaller than 1 is speculative. If the magnitude of the evaporation events caused by the incoming molecules is similar to what it is for water, the number of scattered molecules could outnumber the evaporated by a clear margin. On the other hand, it might be that the exchange evaporation is also enhanced in these situations. For accommodation of a molecule on a surface that consists of a different molecular species, it seems natural to only take into account the fate of the incoming molecular species when calculating the mass accommodation coefficient, even if the adsorption leads to an increase in the evaporation of the surface species.

While it might seem worthwhile to use the sorption layer also when determining α_m , the fact that the MD sorption layer is here so removed from the condensed phase makes it ill-suited for the task. According to the definitions in section 2.4, an incoming molecule that has passed through the surface is classified as absorbed into the bulk liquid, but from Figure 6 it is clear that any molecule that has just traveled past the MD sorption layer can hardly be considered to reside in the bulk liquid phase.

4. CONCLUSIONS

We have performed molecular dynamics simulations of water mass accommodation on both planar and droplet surfaces as well as evaporation simulations with the same set of simulation conditions. These included a planar surface at four different temperatures and droplets at $T = 273.15$ K with radii of 1.92 and 4.14 nm, with the latter size considered in the mass accommodation simulations only. Our simulated water evaporation rates are in qualitative agreement with the evaporation rate given by simple kinetic condensation equations, but this theoretical expression consistently underestimates the observed rates. While a longer simulation time might result in a better quantitative agreement, the systematic difference between the two makes this doubtful. On the other hand, a change of a few hundred pascals in the equilibrium vapor pressure would be needed to bring the theoretical prediction to the same level as simulations.

In the two highest of the studied temperatures, $T = 290$ K and $T = 300$ K, the evaporation rate in the MD mass accommodation simulations is elevated compared to the evaporation simulations. This effect can be attributed to exchange evaporation; that is, an incoming molecule will remain in the condensed phase but causes a surface molecule to evaporate. Such behavior is at odds with the commonly used assumption that the evaporation mass flux is independent of the condensational mass flux, but it should be noted that the relatively frequently generated incident molecules cause the

simulation conditions to correspond to very high supersaturations of the order 10–200. The comparison of MD evaporation rates and theoretical free molecular regime evaporation rates suggests that the evaporation coefficient for water is unity, which is in agreement with earlier MD work where the evaporation coefficient has been calculated from the evaporation fluxes in liquid–vapor equilibrium and vacuum evaporation simulations.²⁶ This is at odds, however, with experimental Raman thermometry results, which point to a value below unity.¹⁶

The MD simulations also provided an opportunity to refine the average desorption lifetime that is required as an input parameter for the detailed kinetic flux model KM-GAP.²³ Using the surface coverage of the KM-GAP sorption layer, the region in the MD simulations that corresponds to this KM-GAP sorption layer is identified. From the time that evaporating molecules spend in this region, we find the average desorption lifetime to be around 1 ps. Although this new τ_d differs by an order of magnitude from the earlier value used in KM-GAP, the model succeeds in describing the condensational growth of water droplets from the experiments of ref 10. In fact, the droplet growth is described equally well with desorption lifetimes ranging from 1 to 100 ps, indicating that the growth is limited by gas phase diffusion and surface accommodation rather than desorption. Thus the simple kinetic treatment (see Figure 1, left panel) is sufficient for describing pure water. This is likely not the case for a situation where the transport between surface and bulk is less efficient, for example, for a water droplet coated with organic molecules.²⁰

A mass accommodation coefficient between 0.99 and 1 is found for all studied planar interfaces, which is in accordance with previous MD studies. Using a droplet as the target surface also produces a coefficient that is practically unity, even though the coefficient appears to get slightly (<0.5%) lower as the droplet radius decreases. The mass accommodation coefficient gets slightly (~0.2%) smaller as temperature increases, which is in agreement with experiments.^{8,9,37} When the exchange evaporation is taken into account, the decrease with increasing temperature is somewhat more pronounced, resulting in a value of 0.99 at the highest temperature. The effect of exchange evaporation is included by comparing the evaporation fluxes in mass accommodation and evaporation simulations and attributing the difference to molecules evaporated by the exchange method and, consequently, as nonaccommodated.

The molecular level definitions of the mass accommodation coefficient conventionally used in MD consider only the fate of the incoming molecules. However, when kinetic condensation models for aerosol growth are used, the picture is not a molecular level one but instead is one of mass fluxes, and then the mass accommodation coefficient acts as a factor that effectively decides the magnitude of the condensation and evaporation fluxes. In this case, the information that the coefficient is expected to contain includes the possible exchange evaporation.

AUTHOR INFORMATION

Corresponding Author

*E-mail: jan.julin@itm.su.se.

Notes

The authors declare no competing financial interest.

ACKNOWLEDGMENTS

This work was supported by the European Research Council ATMOGAIN (No. 278277). We thank PDC Center for high performance computing for the computational resources. M.S. is supported by the Japan Society for the Promotion of Science (JSPS) Postdoctoral Fellowship for Research Abroad. R.E.H.M. acknowledges support from the NERC for a postdoctoral fellowship, and J.P.R. acknowledges the EPSRC for support through a Leadership Fellowship.

REFERENCES

- (1) Rosenfeld, D. *Science* **2000**, *287*, 1793.
- (2) Clement, A. C.; Burgman, R.; Norris, J. R. *Science* **2009**, *325*, 460.
- (3) Fountoukis, C.; Nenes, A. *J. Geophys. Res.* **2005**, *110*, D11212.
- (4) Asa-Awuku, A.; Nenes, A. *J. Geophys. Res.* **2007**, *112*, D22201.
- (5) Barahona, D.; West, R.; Stier, P.; Romakkaniemi, S.; Kokkola, H.; Nenes, A. *Atmos. Chem. Phys.* **2010**, *10*, 2467.
- (6) Kolb, C. E.; Cox, R. A.; Abbatt, J. P. D.; Ammann, M.; Davis, E. J.; Donaldson, D. J.; Garrett, B. C.; George, C.; Griffiths, P. T.; Hanson, D. R.; Kulmala, M.; McFiggans, G.; Pöschl, U.; Riipinen, I.; Rossi, M. J.; Rudich, Y.; Wagner, P. E.; Winkler, P. M.; Worsnop, D. R.; O'Dowd, C. D. *Atmos. Chem. Phys.* **2010**, *10*, 10561.
- (7) Seinfeld, J. H.; Pandis, S. N. *Atmospheric Chemistry and Physics: From Air Pollution to Climate Change*; John Wiley: Hoboken, NJ, 1998.
- (8) Li, Y. Q.; Davidovits, P.; Shi, Q.; Jayne, J. T.; Kolb, C. E.; Worsnop, D. R. *J. Phys. Chem. A* **2001**, *105*, 10627.
- (9) Winkler, P. M.; Vrtala, A.; Wagner, P. E.; Kulmala, M.; Lehtinen, K. E. J.; Vesala, T. *Phys. Rev. Lett.* **2004**, *93*, 075701.
- (10) Winkler, P. M.; Vrtala, A.; Rudolf, R.; Wagner, P. E.; Riipinen, I.; Vesala, T.; Lehtinen, K. E. J.; Viisanen, Y.; Kulmala, M. *J. Geophys. Res.* **2006**, *111*, D19202.
- (11) Davis, E. J. *Atmos. Res.* **2006**, *82*, 561.
- (12) Miles, R. E. H.; Knox, K. J.; Reid, J. P.; Laurain, A. M. C.; Mitchem, L. *Phys. Rev. Lett.* **2010**, *105*, 116101.
- (13) Miles, R. E. H.; Reid, J. P.; Riipinen, I. *J. Phys. Chem. A* **2012**, *116*, 10810.
- (14) Cappa, C. D.; Drisdell, W. S.; Smith, J. D.; Saykally, R. J.; Cohen, R. C. *J. Phys. Chem. B* **2005**, *109*, 24391.
- (15) Smith, J. D.; Cappa, C. D.; Messer, B. M.; Drisdell, W. S.; Cohen, R. C.; Saykally, R. J. *J. Phys. Chem. B* **2006**, *110*, 20038.
- (16) Smith, J. D.; Cappa, C. D.; Drisdell, W. S.; Cohen, R. C.; Saykally, R. J. *J. Am. Chem. Soc.* **2006**, *128*, 12892.
- (17) Cappa, C. D.; Smith, J. D.; Drisdell, W. S.; Saykally, R. J.; Cohen, R. C. *J. Phys. Chem. C* **2007**, *111*, 7011.
- (18) Morita, A.; Sugiyama, M.; Kameda, H.; Koda, S.; Hanson, D. R. *J. Phys. Chem. B* **2004**, *108*, 9111.
- (19) Vieceli, J.; Roeselová, M.; Potter, N.; Dang, L. X.; Garrett, B. C.; Tobias, D. J. *J. Phys. Chem. B* **2005**, *109*, 15876.
- (20) Takahama, S.; Russell, L. M. *J. Geophys. Res.* **2011**, *116*, D02203.
- (21) Neshyba, S.; Nugent, E.; Roeselová, M.; Jungwirth, P. *J. Phys. Chem. C* **2009**, *113*, 4597.
- (22) Vesala, T.; Kulmala, M.; Rudolf, R.; Vrtala, A.; Wagner, P. E. *J. Aerosol Sci.* **1997**, *28*, 565.
- (23) Shiraiwa, M.; Pfrang, C.; Koop, T.; Pöschl, U. *Atmos. Chem. Phys.* **2012**, *12*, 2777.
- (24) Pöschl, U.; Rudich, Y.; Ammann, M. *Atmos. Chem. Phys.* **2007**, *7*, 5989.
- (25) Matsumoto, M. *Fluid Phase Equilib.* **1998**, *144*, 307.
- (26) Ishiyama, T.; Yano, T.; Fujikawa, S. *Phys. Fluids* **2004**, *16*, 4713.
- (27) Hess, B.; Kutzner, C.; van der Spoel, D.; Lindahl, E. *J. Chem. Theory Comput.* **2008**, *4*, 435.
- (28) Horn, H. W.; Swope, W. C.; Pitera, J. W.; Madura, J. D.; Dick, T. J.; Hura, G. L.; Head-Gordon, T. *J. Chem. Phys.* **2004**, *120*, 9665.
- (29) Bussi, G.; Donadio, D.; Parrinello, M. *J. Chem. Phys.* **2007**, *126*, 014101.
- (30) Hirschfelder, J. O.; Curtiss, C. F.; Bird, R. *Molecular Theory of Gases and Liquids*; John Wiley & Sons: New York, 1964.

- (31) Vehkamäki, H.; Riipinen, I. *Chem. Soc. Rev.* **2012**, *41*, 5160.
- (32) Fuchs, N. A.; Sutugin, A. G. In *Topics in Current Aerosol Research (Part 2)*; Pergamon: New York, 1971; pp 1–200.
- (33) Roeselová, M.; Jungwirth, P.; Tobias, D. J.; Gerber, R. B. *J. Phys. Chem. B* **2003**, *107*, 12690.
- (34) Vega, C.; Abascal, J. L. F.; Nezbeda, I. *J. Chem. Phys.* **2006**, *125*, 034503.
- (35) Sakamaki, R.; Sum, A. K.; Narumi, T.; Yasuoka, K. *J. Chem. Phys.* **2011**, *134*, 124708.
- (36) Garrett, B. C.; Schenter, G. K.; Morita, A. *Chem. Rev.* **2006**, *106*, 1355.
- (37) Davidovits, P.; Worsnop, D. R.; Jayne, J. T.; Kolb, C. E.; Winkler, P.; Vrtala, A.; Wagner, P. E.; Kulmala, M.; Lehtinen, K. E. J.; Vesala, T.; Mozurkewich, M. *Geophys. Res. Lett.* **2004**, *31*, L22111.
- (38) Nagayama, G.; Tsuruta, T. *J. Chem. Phys.* **2003**, *118*, 1392.